NOVEMBER 1981 PPPL-1856
UC-20G

TRANSPORT OF MOLECULAR IMPURITIES AT THE EDGE OF TOKAMAKS

BY

WILLIAM D. LANGER

PLASMA PHYSICS LABORATORY

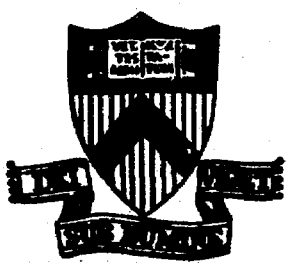

PRINCETON UNIVERSITY
PRINCETON, NEW JERSEY

This work was supported by the U.S. Department of Energy Contract No. DE-AC02-76-CHO 3073. Reproduction, translation, publication, use and disposal, in whole or in part, by or for the United States government is permitted.

TRANSPORT OF MOLECULAR IMPURITIES AT THE EDGE OF TOKAMAKS

William D. Langer

Plasma Physics Laboratory, Princeton University

Princeton, New Jersey 08544

ABSTRACT

The transport of molecules at the plasma edge in tokamaks is discussed in order to compare how light impurities enter the plasma if they are released either in atomic or molecular forms. Differences in their transport arise because of the dissimilarities between the atomic and molecular reactions with the bulk of the plasma. It is found that recycling to the walls is more efficient for the light impurities released in molecular form, but, also, that a substantial fraction of those atoms which originate from molecules may penetrate further into the plasma.

1. INTRODUCTION

It is important to understand the transport of impurities, such as carbon and oxygen, since these affect both the cooling (at the edge) and the associated stability of the plasma. Light ion impurities can enter a plasma from the wall or limiter as molecules as well as atoms. The purpose of the investigation described here is to elucidate the mechanisms peculiar to molecules which affect their transport, and to explore the differences in the transport of an impurity if it leaves the wall in either atomic or molecular form. Differences in the transport of molecular and atomic species are due to their different reactions with the bulk of the plasma. In particular, the examples of carbon and methane will be analyzed for a simple one-dimensional model in which their transport is followed from release until C^+ is produced. The results have application to recycling studies, divertor design, and transport analysis.

In magnetically confined plasmas, molecules and molecular impurities are present either as products of plasma-surface interactions, or as probes which have been introduced to study impurity transport. The role of molecules and molecular reactions has been appreciated in the case of recycling of hydrogen from the walls [1] (see also the review paper by McCracken and Stott [2]), where the reactions of molecular hydrogen are known to be more complex than those of atomic hydrogen.

In a plasma-surface interaction, chemical reactions occur in which an incident atom or ion reacts with a surface atom to form a molecule. The presence of a carbon surface in a hydrogen plasma, for example, results in the formation of methane [3]. Beam experiments involving hydrogen impinging on carbon produce both methane and acetylene [4] with the latter molecule favored at high temperatures. Furthermore, Dylla et al. [5] have found that during

glow discharge cleaning, carbon is removed from stainless steel and titanium surfaces by the formation of methane (the methane is readily desorbed from the surface because it has a low binding energy). There is evidence also that oxygen bearing molecules, such as water, can be produced at the wall (see the summary by McCracken and Stott). Finally, molecular impurities, such as silane and methane, have been introduced into plasmas by gas puffing in order to study transport [6].

To explore the transport of molecular impurities, a simple one-dimensional model has been used which includes the processes relevant to molecules and molecular ions in a plasma. The density distributions and source functions for the molecular and atomic products are calculated as a function of the plasma properties near the edge. The emphasis here is on elucidating the differences between atomic and molecular transport of impurities. Methane is the molecular species chosen for study for three reasons: (1) it is observed to form in tokamaks as a consequence of plasma surface interactions; (2) it is a molecule some of whose reactions with ions and electrons have been studied in the laboratory, and, (3) it is the chemical analog of silane which is used extensively in impurity transport experiments (Meade, D., and Burrell, K., private communication).

The analysis here indicates that there are qualitative and quantitative differences in the transport of atomic and molecular impurities at the edge. The details of the atomic and molecular processes within the plasma are found to be very important for the analysis of the transport of neutral and molecular ions. The most significant differences in the transport are: (1) roughly half of the carbon released from methane, due to its breakup, returns to the wall (or limiter), and (2) the remaining carbon derived from the breakup of methane penetrates further into the plasma before it is ionized

than would a corresponding carbon atom released at the wall. The conclusions reached here for methane versus carbon transport hold for some other pairs as well (such as, silane and silicon) and are a general feature of the differences between atomic and molecular transport. The case of water and oxygen is slightly different, however, from carbon and methane because of the charge exchange reactions of oxygen with protons.

The outline of this paper is as follows. In Section II, the key molecular processes are reviewed (details are left to the Appendix); the transport model is presented in Section III, and the results of several transport calculations for different density and temperature profiles are discussed in Section IV along with their relevance to recycling, scrapeoff, and impurity injection.

2. MOLECULAR PROCESSES AND TRANSPORT

There is a variety of collisional processes which are important for establishing the transport of atoms and molecules. At the plasma edge, a neutral launched at the wall (or limiter) travels unaffected by the magnetic fields. Once it is ionized, an atom's density distribution in the plasma can be determined by solving a transport equation including ionization and recombination processes along with various diffusion terms [7]. The emphasis here will not be on the transport and distribution of the ionized states of carbon throughout the plasma, but rather to determine the source function of singly ionized carbon which arises from the transport of methane. The goal, in part, is to describe the distribution of neutral and singly ionized carbon at the edge of the plasma where the source at the wall is either carbon (atom) or methane (molecule).

The variety of collisional processes which determine the distribution of

atomic carbon at the plasma edge is relatively small. Carbon is ionized almost entirely by collisions with electrons, $e + C \rightarrow C^+ + 2e$, (Table I), since ionization or charge exchange in collisions with protons is comparatively slow. Carbon ions are destroyed also by electrons, either by recombination ($C^+ + e \rightarrow C + h\nu$) or collisional ionization ($e + C^+ \rightarrow C^{++} + 2e$).

In contrast to the destruction of carbon, the number of collisional processes which must be considered for methane and its derivatives is large. Its interaction with electrons can result in ionization ($e + CH_4 + CH_4^+ + e$), dissociative ionization ($e + CH_4 \rightarrow CH_3^+ + H + 2e$, plus other channels), and dissociation ($e + CH_4 \rightarrow CH_3 + H + e$, plus other channels). Unlike the situation for atomic carbon, protons do charge exchange rapidly with methane. This exchange reaction can have a profound effect on the methane distribution because, unlike the reactions with electrons, it is exothermic. Therefore, in a low temperature plasma where collisional ionization by electrons is slow, carbon is not readily ionized while methane is efficiently ionized due to charge exchange. These reactions are summarized in Table I, and their rate constants plotted in Fig. 1.

The subsequent evolution of methane ions (or of its radicals, such as CH_3^+) depends on the electrons and protons in the plasma. The electrons are responsible for destroying the ions by collisional dissociation (e.g., $e + CH_4^+ \rightarrow CH_3^+ + H + e$) or dissociative recombination ($e + CH_4^+ \rightarrow CH_3 + H$, etc.), while the protons transfer kinetic energy to the ions. The product ions and neutrals are destroyed themselves by reactions with electrons through channels analogous to those described for CH_4 and CH_4^+.

A crucial stage in the degradation of methane into atomic components occurs when only CH^+ remains. This ion can recombine dissociatively,

$$e + CH^+ \rightarrow C + H,$$

or be collisionally dissociated,

$$e + CH^+ \rightarrow C^+ + H + e$$
$$\rightarrow C + H^+ + e,$$

with nearly equal reaction rates for these last two channels. Therefore, a significant fraction of the methane will appear as a source of neutral carbon inside the plasma. This dissociation results in a different distribution of carbon within the plasma and, consequently, a different source of C^+ from that due to carbon atoms leaving the wall. The distribution of the flux of carbon from this molecular source also is quite unlike that due to an atomic source, since the carbon produced from CH_4 destruction moves in all directions, and some flux is directed towards the wall.

Another distinction between the transport of atomic and molecular impurities results from the interaction of protons with molecular ions. The energy of the methane launched at the wall will be lower than that of the plasma ions. Collisions of energetic protons will accelerate the methane ion and its derivatives, CH_n^+. Whether they come to thermal equilibrium or not depends on the equilibration time and the lifetime of the ion. This equilibration process is extremely important because the carbon produced is more energetic than the original methane. In effect, the methane becomes a source of energetic neutral carbon away from the edge, and this energetic carbon can penetrate deeper into the plasma or return to the wall.

To summarize this part of the discussion, methane is degraded by interactions with both electrons and protons and introduces a source of

neutral carbon in the plasma. A sample sequence of reactions is:

$$e + CH_4 \rightarrow CH_3^+ + H + e$$
$$e + CH_3^+ \rightarrow CH_2^+ + H + e$$
$$e + CH_2^+ \rightarrow CH^+ + H + e$$
$$e + CH^+ \rightarrow C + H .$$

Thermal equilibration of molecular ions by protons results in energetic neutrals being produced in the plasma. Thus, the distribution transport and shielding of impurities may be quite different for atomic and molecular sources.

3. TRANSPORT MODEL

To determine quantitatively the impurity distribution in the plasma near the wall, a simple transport model was adopted in which each of the molecular and atomic components is treated separately. In this approximate solution, the source function of molecular ions throughout the plasma must be found for a given flux of neutral molecules from the wall. Next, the fraction that appears as neutral impurity atoms, as a result of collisional destruction of the molecular ions, is determined. The source function of neutral atoms throughout the plasma must then be calculated after including the effects of the equilibration processes. The transport of these energetic neutrals arising from throughout the edge is then calculated, and a source function of atomic ions determined. These processes, the corresponding equations, and approximations are described step-by-step below.

First, the impurity density of the molecules leaving the wall $n(x)$ is determined from a one-dimensional transport equation

$$\frac{\partial n(x)}{\partial t} = - \frac{\partial \Gamma(x)}{\partial x} + S(x) - \Lambda(x)\, n(x) \ , \qquad (1)$$

where Γ is the flux and S the source of the impurity. The term Λ is the loss rate due to collisional destruction of the impurity; no mechanism for production of molecular impurities is included although, obviously, atoms returning to the wall may catalyze into molecules. The source function at the wall, $S(x=o)$, is assumed to produce particles with a constant velocity characterized by the average thermal velocity corresponding to a temperature T_M. The source function has the form,

$$S_M^{in}(x) = n_M v_M^{in}\, \delta(x-o), \qquad (2)$$

where M denotes molecule and the superscript "in" indicates transport into the plasma, ("out" is used to label transport back towards the wall). In steady state, these equations have the simple solution

$$n_M^{in}(x) = n_M^{in}(o)\, \exp\left(-\int_o^x \frac{dx'}{\lambda(x')}\right) \ , \qquad (3)$$

where $\lambda(x') = \Lambda(x')/v_M(x')$, and the loss term $\Lambda = n_e \Sigma \langle \sigma v \rangle_i + n_p \Sigma \langle \sigma v \rangle_i$. The flux of molecules is given by $\Gamma_M^{in}(x) = n_M^{in}(x)\, v_M^{in}(x) = n_M^{in}(x)\, v_M^{in}(o)$ assuming the velocity is unchanged.

Once the molecule is ionized, it is trapped by the magnetic fields, and, to a good approximation transport across field lines, can be neglected. This approximation is possible because the destruction of the molecular ion is rapid, and its diffusion velocity is so small that transport across field lines is insignificant during this time. (Of course, transport along field lines occurs; however, as discussed in Section IV, this is not important for

the discussion here.) The ion transport equation is

$$\frac{\partial n_I(x)}{\partial t} = - \frac{\partial \Gamma_I(x)}{\partial x} + \Pi(x) - \Lambda(x)\, n_I \,, \tag{4}$$

where Π is the production rate. In steady state, since perpendicular transport is not allowed ($\Gamma_I = 0$), the ion density is given by

$$n_I(x) = \Pi(x)/\Lambda(x)$$

$$n_I(x) = n_M(x) \frac{\Sigma \{n_e \langle \sigma v \rangle_i + n_p \langle \sigma v \rangle_i\}}{n_e \Sigma' \langle \sigma v \rangle_i}, \tag{5}$$

where Σ denotes the sum over ionization terms for M and Σ' destruction terms for $I = M^+$.

The destruction of a molecular ion, such as CH_4^+, produces either another ion or a neutral (e.g., CH_3^+ or CH_3) with the former process dominating above 6 eV. The proliferation of neutral and ionic species complicates the treatment of molecular transport since a multispecies formulation is required. To make this problem tractable within the scope of this paper, it is assumed that the destruction of an ion, CH_n^+, generates only another ion if $n \geq 2$. (For the plasma profiles considered in Section III, this is a good approximation since the molecular ions form in regions where the electron temperature is larger than 6 eV and, hence, where the destruction produces primarily ions.) During the time when the impurities exist as ions, their transport across field lines can be neglected compared to the transport during their neutral phase. Thus, in the scheme used here, one CH_4^+ is produced, and it is broken down subsequently as follows, $\rightarrow CH_3^+ \rightarrow CH_2^+ \rightarrow CH^+$. To a good approximation, the destruction rates of all these species are equal and the

following relationship holds:

$$n(CH_{n-1}^{+}) = n(CH_n^{+}) \ . \tag{6}$$

Finally, the simplest molecular ion CH^+ is broken up into C and C^+.

The net effect of all these processes is to produce a source function of neutral carbon which is proportional to that for CH_4^+,

$$S_C(x) = \beta \, S_{CH_4^+}(x) \ , \tag{7}$$

where β is the branching ratio to carbon,

$$\beta = \frac{\langle \sigma v \rangle_{8+9}}{\langle \sigma v \rangle_{7+8+9}} \ , \tag{8}$$

and the numbers refer to the reactions in Table I. At temperatures less than 4 eV, recombination dominates the destruction of CH^+ and $\beta \simeq 1$. Above 10 eV, the factor β depends critically on the branching of the collisional dissociation channels (reactions 7 and 8 in Table I).

Before continuing with a description of the transport of the neutral carbon produced by the destruction of methane, it is important to consider the equilibration of the molecular ions in the plasma. Collisions between protons and molecular ions will transfer energy from the plasma to the impurities raising the temperature of the molecular ions. The extent of the thermalization depends on the equilibration time versus the lifetime of the molecular ion (it is in this stage that equilibration proceeds most rapidly). The ion-ion thermal equilibration process is outlined below.

For a test particle streaming through a background of field particles,

the energy loss (or gain) is

$$\frac{d\varepsilon}{dt} = -\nu_{\varepsilon}^{p}\,\varepsilon_{p}\ , \tag{9}$$

where ν_E is the energy transfer rate defined in the NRL Tables [8]

$$\nu_{\varepsilon} = 6.8 \times 10^{-8}\,\frac{n_p \lambda}{T^{1/2}}\,\frac{\mu_p^{1/2}}{\mu_{CH_4}}\left\{\frac{2}{T}\left(1 + \mu_p/\mu_{CH_4}\right) - \frac{3}{\varepsilon}\right\}\ , \tag{10}$$

λ is a screening factor, and μ is the mass in atomic units. For the conditions considered here $\lambda \approx 10$ and $\nu_{\varepsilon} \approx 8.8 \times 10^{-8}\ n_p T_p^{-3/2}\ s^{-1}$. Solving the equation for $d\varepsilon/dt$ yields

$$\varepsilon_{CH_4}(t) = \varepsilon_{CH_4}(o)\,\exp\left(-t/\tau_q\right) + \varepsilon_p\left(1 - \exp(-t/\tau_q)\right)\ , \tag{11}$$

where the equilibrium time $\tau_q = 1.1 \times 10^7\ T_p^{3/2}/n_p$ sec.

The amount of energy the molecular ions gain depends on their lifetime, and the final energy ε is determined by setting $t \approx 4\tau$ (τ is the lifetime of an ion) since it takes roughly four stages of destruction to go from CH_4^+ to C. Most of the equilibration energy goes into the carbon atom because the center of the mass of the molecular ion is nearly coincident with the carbon due to its large mass. The energy transferred to the carbon atom during the destruction process, due to the excitation energy required to dissociate in the Franck-Condon region, is small since most of the energy goes into the lighter hydrogen(s). Accordingly, this dissociation energy is neglected.

The destruction and equilibration rate constants are plotted in Fig. 2 as a function of temperature assuming $n_e = n_p$. These curves cross at 4 eV so that at higher energies equilibrium is not reached. At these higher energies,

however, even a short time interval is sufficient to increase the energy of the molecular ion substantially since in the regime where $t/\tau_q << 1$ the energy ε_p is large, $\varepsilon_p >> \varepsilon_{CH_4}(t=o)$.

To determine the transport of the energetic neutral atoms, a transport equation more complicated than that for the molecules must be solved. For every position x there are energetic neutrals, generally, with different energies (and velocities) produced in all directions. At each point x then, the following transport equation applies in steady state

$$\frac{\partial \Gamma_C^a}{\partial x}(x,E) + \frac{\Lambda(x,E)}{v(x)} \Gamma_C^a(x,E) = S_C^a(\xi,E)\ \delta(x-\xi)\ , \qquad (12)$$

where E, the energy of the carbon atoms, is determined by Equation (11) at the position of the source function ξ. The label a denotes either 'in' or 'out', and Λ is the ionization rate of carbon (recombination of C^+ is excluded as a source of C). The total flux, at each point, is determined by summing over all positions which are sources of flux in the appropriate direction; this yields

$$\Gamma^{in}(x) = \int_o^x S^{in}_{CH_4^+ \to C}(x') \exp\left(-\frac{1}{v(x')} \int_{x'}^x \Lambda(\xi)\ d\xi\right) dx'\ , \qquad (13)$$

$$\Gamma^{out}(x) = \int_x^{x_{max}} S^{out}_{CH_4^+ \to C}(x') \exp\left(-\frac{1}{v(x')} \int_{x'}^{x'} \Lambda(\xi)\ d\xi\right) dx'\ , \qquad (14)$$

where $S^{in} + S^{out} = \beta\, S_{CH_4^+}$ (the label E has been suppressed). (In this one-dimensional model, particles passing through x towards the center originate between the wall and x, while those going towards the wall originate between x and the center of the plasma, x_{max}.) The source function of C^+ in the plasma can be determined as follows:

$$S_{C^+}(x) = S_{CH^+ \to C}(x) + \Lambda(x)\, n_C(x) \quad , \tag{15}$$

where the contributions are the direct production of C^+ from the breakup of CH^+ and the ionization of carbon. This latter term can be derived from Equation (12) by expressing Γ in terms of nv, using the assumption that E is single valued at ξ, solving for n(x,E), and then averaging over all energies

$$n_C(x)\Lambda_C(x) = -\frac{\partial \Gamma_C(x)}{\partial x} + S_{CH^+ \to C}(x) \quad ,$$

which yields

$$S_{C^+}(x) = S_{CH^+}(x) - \frac{\partial \Gamma_C(x)}{\partial x} \quad , \tag{16}$$

where $S_{CH^+}(x)$ is the total source function for the production of CH^+ (= $S_{CH_4^+}(x)$ under the assumptions adopted here.)

4. RESULTS AND DISCUSSION

The one-dimensional transport model has been solved using equations 3, 5-8, 10, 11, and 13-16, and the results have been used to compare the transport of methane and carbon from the wall into the plasma. Two different plasma profiles were chosen - one determined theoretically and one experimentally. The theoretical profile, called Model 1, is discussed by Hawryluk, Suckewer, and Hirshman [7], and is characterized by a high central density (7×10^{13} cm^{-3}) and electron temperature (1400 eV); the profiles have been calculated with the BALDUR code [9]. The second model is based on probe measurements [10] of the edge in PDX for a standard diverted plasma with some extrapolation to

merge with measurements inside the edge. The electron and proton densities and temperatures for the outer part of these profiles are shown in Fig. 3. The impurity transport for a range of initial energies is discussed below.

The impurity density distributions for C and CH_4 leaving the wall are shown in Fig. 4 for these two profiles assuming a temperature for the impurities at the wall of 0.03 eV. The cases for carbon and methane are evaluated for equal fluxes leaving the wall (because the velocity of the carbon is slightly higher at the wall than that of methane, and its number density is correspondingly lower at the wall). Neither the carbon nor methane is attenuated significantly until the column density of the plasma is about a few x 10^{12} cm^{-2}. The carbon atoms leaving the wall penetrate slightly further into the plasma than the methane molecules since the atoms are destroyed only by the electrons.

The difference between the penetration of carbon and methane is evident also in the source functions of the first ionization, $S(A^+,E_o)$ shown in Fig. 5 where A denotes the species. The peak of S_{C^+} occurs about 3 cm further into the plasma than that of $S_{CH_4^+}$ as summarized in Table II. These ions are produced over a few cm of the plasma as indicated by the width of the source functions.

As described in Section III, the flux of energetic carbon produced from CH_4 can be calculated from $S_{CH_4^+}$ and can be expressed in terms of a component into the plasma, Γ^{in}, and one towards the wall, Γ^{out}. These fluxes are plotted for the two models in Fig. 6. The flux into the plasma is peaked 2 to 3 cm further in than the maximum for $S_{CH_4^+}$; it decreases near the wall because the source of CH_4^+ vanishes there and decreases towards the interior because the carbon is ionized rapidly. The flux out of the plasma, in contrast, reaches a maximum at the wall and is fairly flat at the edge. Thus

the carbon atoms launched back towards the wall are (essentially) unattenuated since the electron temperature and column density in this direction are too low to destroy the carbon.

The source function of energetic carbon ions, $S_{C^+}(E_f)$, can be calculated from the ionization of energetic carbon atoms and the direct production of C^+ from CH^+ as shown in Fig. 5. This source function has two local maxima, one is close to the peak in $S_{CH_4^+}$ and comes from the direct production of C^+ from the breakup of CH^+. The magnitude of this peak depends on the branching ratio β [Eq. (8)], which is different in the two models considered owing to the temperature dependence of reactions 7-9. The second corresponds to the ionized carbon atoms launched in the plasma. Compared to the peak in $S_{CH_4^+}$, the second peak, or $S_{C^+}(E = E_f)$, is 6 to 10 cm further into the plasma. In all cases considered here, this source function peaks further into the plasma than that for carbon launched at the walls. The difference in the position of the maxima of S_{C^+} is 2 to 4 cm (Table II) with the largest value for Model 2 (the measured profile). It is of importance also to note that the source function in this model is very wide and flat so that a significant fraction of the carbon ions are transported up to 10 cm further into the plasma compared to the case of carbon launched from the walls. In all these cases, the value of the source function of energetic C^+ is smaller than that for the slow C^+ (carbon originating at the walls) because only a fraction (here 0.5) of the energetic carbons produced from CH_4^+ travels towards the center. The energetic carbon atoms and ions, produced in the plasma, have energies typically in the range 1.5 to 3.0 eV, considerably larger than the input energy at the wall (0.03 eV).

While the calculation here was restricted to one dimension, it is useful to consider how far the molecular ions might travel down the field lines since

that determines where the neutral atoms will return to the wall. In Table II are listed the maximum distances of travel for a molecular ion during its lifetime if its velocity were the value it has at the end of its acceleration by the equilibration process (i.e., its maximum value). The maximum toroidal distance ranges from 16 to 24 cm so that the carbon that is produced from the CH_4^+ should return to the walls close to the point of origin, in agreement with observations on PLT [11]. To determine the fraction of CH_4^+ which appears as energetic C^+ in the plasma, the integrated source functions, $\int S(x)\,dx$, have been determined for $S_{CH_4^+}$ and $S_{C^+}(E = E_f)$. The fraction of carbon ions, $S_{CH^+}(E = E_f)/S_{CH_4^+}$, is 0.65 and 0.55 for Models 1 and 2 respectively. Correspondingly, this indicates that 35 to 45 percent of the carbon returns to the wall in atomic form in a one-dimensional model of the transport.

The energy with which molecules leave the wall or limiter is likely to be in the range 0.03 to 0.1 eV [12]. Calculations of the transport at 0.1 eV yield qualitatively similar results to those at 0.03 eV (discussed above) except that the peaks of the source functions are shifted ~ 1 cm further into the plasma for both Models 1 and 2.

Shielding studies in PDX [6] have been made by sequentially injecting silane (SiH_4) by gas puffing and atomic silicon by laser ablations. In these studies, the former had an energy E ≈ 0.025 eV, close to the value used in the examples in this paper for methane, but the latter had a considerably higher energy, E ≈ 5 eV. The transport of silane and silicon should be similar to that of methane and carbon. To model the experimental situation, an energy at the wall of 5 eV was adopted for the transport calculation for carbon. In Table III are listed the positions where the source function of C^+ is a maximum for 5 eV carbon leaving the wall. In both models, it can be seen that

these 5 eV carbon atoms penetrate slightly further than those carbon atoms produced from 0.03 eV methane. While the position of maximum source functions of C^+ are similar, the magnitudes are quite different since nearly half the low energy carbon is returned to the walls. Thus the experiments using silicon and silane should find better shielding of silane than silicon.

The analogy silicon (silane) and carbon (methane) does not hold for oxygen (water), primarily because oxygen charge exchanges rapidly with protons. To account for this effect requires a more complicated transport model than the one adopted here.

Three major conclusions arise from the calculations of molecular impurity transport:

(1) the production of molecular impurities at the wall results in an increased penetration depth of atomic impurities into the plasma;

(2) roughly half of these heavy impurity atoms return to the wall. The net effect is that fewer impurity atoms penetrate the plasma, but those that do penetrate further;

(3) the carbon returns to the wall close to the source of molecules.

A number of studies utilizing impurity injection are in agreement with the analysis presented here. Injection of methane into PLT has resulted in the return of substantial amounts of carbon near the point of injection in accord with conclusions 2 and 3.

ACKNOWLEDGMENTS

The author would like to thank R. Budny, S. Cohen, D. Post, J. Schmidt, C. Singer, and J. Weisheit for their comments and A. Silverman for assisting with the computer models.

This work was supported by the U. S. Department of Energy Contract No. DE-AC02-76-CH0-3073.

APPENDIX A

The cross sections and rate constants for collisional processes with molecules and molecular ions are discussed here for the range of energies important at the edge of the plasma. The total number of processes that must be considered when all the molecules and molecular ions (CH_n and CH_n^+) are included is large. Only the most important of these will be considered in any detail. In general, reactions involving CH_4 and CH_4^+ have been studied in the laboratory to a greater extent than their corresponding free radicals (e.g., CH_3, CH_2, and CH). The reactions with these subunits are sufficiently similar to those for CH_4 that estimates can be made of the cross sections and rate constants from the methane data.

Electron collisions ionize and dissociatively ionize methane leading to the following channels:

$$\begin{aligned} e + CH_4 &\rightarrow CH_4^+ + 2e \\ &\rightarrow CH_3^+ + H + 2e \\ &\rightarrow CH_n^+ + \text{products of H} + 2e \\ &\rightarrow C + H^+ + \text{products of H} + 2e. \end{aligned} \qquad \text{(A-1)}$$

The first two channels comprise over 90% of the total ionization cross sections over the range of energies 20 to 2,000 eV [13]. These cross sections can be fit by a functional form similar to that employed by Lotz [14] for collisional ionization of atoms, $\sigma \propto \Sigma\, a_i E^{-1}\, \ln(E/E_i)$ for $E > E_i$. The fits for producing CH_4^+ and CH_3^+ are given in Table I using the branching ratios derived by Adamczyk et al. [13], and scaling the total ionization cross section to agree with the measurements of Rapp and Englander-Golden [15]. The analytic fits are good to better than 35% up to electron energies of 200 eV.

The reaction rate constant for a Maxwellian distribution of the electron velocity must be evaluated numerically. Plots of $\langle \sigma v \rangle$ as a function of the electron temperature determined in this paper are shown in Fig. 1.

Electrons also can dissociate methane into neutral products, and the dominant channels are [16]

$$\begin{aligned} e + CH_4 &\rightarrow CH_3 + H + e \\ &\rightarrow CH_2 + 2H + e. \end{aligned} \qquad (A-2)$$

The total dissociation cross section for methane, that is neutral plus ionic fragments, has been measured by Winters [17] for the energy range 10 to 500 eV. To determine the cross section for dissociation into neutral fragments, the dissociative ionization cross section must be subtracted from the total dissociation cross section measured by Winters. Following this procedure, similar to that discussed by deHeer [18] above 100 eV, we have determined σ above 10 eV. The fit to these values, as given in Table I, are good to within 50% over the range of 10 to 500 eV. In general, various experimental measurements differ by an amount comparable to or more than that of the error of the fits in Table I.

In contrast with electron collisional ionization of methane, the charge exchange with protons,

$$p + CH_4 \rightarrow CH_4^+ + H, \qquad (A-3)$$

is exothermic. At thermal energies, the reaction of protons with CH_4 has another channel leading to $CH_3^+ + H_2$, and the total reaction rate constant for both channels is $\langle \sigma v \rangle = 3.8 \times 10^{-9}$ cm^3 s^{-1} [19] independent of temperature.

This rate implies a value for $\sigma = 1.1 \times 10^{-15}\ E^{-1/2}$ cm^2 for $E \lesssim 1$ eV. Above 40 eV, the primary channel is the charge-exchange reaction, $p + CH_4 \rightarrow CH_4^+ + H$ [20], and above 100 eV it has a nearly constant cross section [σ (100 eV) = 3.8×10^{-15} cm^2] as measured [21]. This cross section is predicted to have a maximum at ~ 50 eV and, for lack of any additional data, a value of 2×10^{-15} cm^2 has been adopted. This value is intermediate between the value at 1 eV (extrapolating the thermal energy measurement) and 100 eV; the corresponding rate constant is given in Table I. In the absence of any laboratory data for CH_3, CH_2, and CH, it is assumed that the cross sections and rate constants for collisional destruction by electrons and protons are the same as those for CH_4.

The molecular ions can be destroyed by recombination and dissociation. The cross sections and energy dependence for dissociative recombination of CH_4^+, CH_3^+, CH_2^+, and CH^+ below 0.08 eV have been measured by McGowan et al. [22] who find a rough E_e^{-1} dependence for σ (there is a slight deviation for CH^+) corresponding to a $T_e^{-1/2}$ dependence for $\langle \sigma v \rangle$. Unfortunately, there are no data for these species at higher energies, and other related molecular systems must be used as a guide. Studies with $C_2H_2^+$ and $C_2H_3^+$ [23] show a continuation of the $\sim E^{-1}$ law up to 1 eV. Experiments above 1 eV with H_3^+ show that the low energy power law no longer holds due to the contribution of excited Rydberg states of the molecule [24]. There is considerable structure in $\sigma(E)$ so that a power law fit can only be a crude estimate; it is found that $\sigma \propto E^{-0.6}$ over the range 1 to 6 eV approximates the general trend of the H_3^+ data. This energy dependence for H_3^+ is adopted as characteristic of that for CH_n^+, and the proportionality constant is that measured for $C_2H_2^+$ at 1 eV. At high energies (E > 10 eV) collisional dissociation is more important than dissociative recombination, and only a small error is introduced in the

transport results by extrapolating the rates to higher energies where they may not be valid.

As the electron energy increases above a few eV, collisional dissociation is the dominant destruction mechanism for molecular ions. The cross sections for this process with CH_4^+ has not been measured, but the branching ratios to various channels have been determined at 70 eV by Tunitskii, Kupriyanov, and Perov [25]. They find that the primary product is $CH_3^+ + H$ (0.75 fraction) followed by $CH_2^+ + 2H$ (0.15 fraction). The cross sections are determined from the related reaction, $e + H_3^+ \rightarrow H^+ + 2H$, which has been studied by Peart and Dolder [26].

For the collisional dissociation of CH^+, it is important to know the relative branching ratio of the two channels,

$$\begin{aligned} e + CH^+ &\rightarrow C^+ + H \\ &\rightarrow C + H^+, \end{aligned} \qquad \text{(A-5)}$$

since this strongly influences the carbon source function in the plasma. The potential energy curves of CH^+ given by Lorquet et al. [27] indicate that states corresponding to dissociation into $C + H^+$ are accessible from the ground state and require an energy comparable to that for $C^+ + H$ in the Franck-Condon region. It seems likely then that these are equally probable.

The dissociative recombination rate for CH^+ is taken to be one-third that for CH_4^+ corresponding to the differences observed at very low energies. The difference is presumably due to the larger number of states accessible to a polyatomic ion.

APPENDIX B

This appendix gives a brief discussion of the collisional processes and reaction rates for atomic carbon. The rate constant for electron collisional ionization has been evaluated by Lotz [28], based on empirical fits to the cross section [14], and should be accurate to within 50% at the energies of interest here (< 100 eV).

Neutral carbon, in marked contrast with methane, does not readily charge exchange with protons. The rate constant for $H^+ + C \rightarrow C^+ + H$ has been calculated to be less than 3×10^{-16} cm^3 s^{-1} at 1 eV by Butler [29]; this is orders-of-magnitude smaller than the collision ionization rate and can, therefore, be neglected.

The recombination rate of carbon ions consists of a radiative part that dominates at low temperatures ($T_e \lesssim 2$ eV) and a dielectronic part at higher temperatures. For both these processes the following analytic forms are used [30]: radiative recombination, $\langle \sigma v \rangle = 4.4 \times 10^{-13} T_e^{-0.624}$ cm^3 s^{-1}; and dielectronic recombination $\langle \sigma v \rangle = 6.0 \times 10^{-10} T_e^{-1.5} \exp(-10/T_e) \times [1 + 3 \exp(-4.5/T_e)]$ cm^3 s^{-1}.

REFERENCES

[1] HOFMANN, F. W., BISHOP, A. S., and HINNOV, E., Princeton Plasma Physics Laboratory Report MATT-305 (1964). McNeill, D. H., Princeton Plasma Physics Laboratory Report MATT-1758 (1981).

[2] McCRACKEN, G. M., and STOTT, P. E., Nuclear Fusion, 19, 889 (1979).

[3] ROSSNER, D. E., ALLENDORF, H. D., in Heter. Kinetics at Elevated Temperatures, Proc. Int. Conf., University of Pennsylvania, Plenum Press, New York (1970).

[4] BALOOCH, M., and OLANDER, D. R., J. Chem. Phys. 63, 4772 (1975).

[5] DYLLA, H. F., COHEN, S. A., ROSSNAGEL, S. M., McCRACKEN, G. M., and STAIB, Ph., J. Voc. Sci. and Tech. 17, 286 (1980).

[6] MEADE, D., et al., Eighth International Conference on Plasma Physics and Controlled Nuclear Fusion Research, Brussels, July 1-10, 1980, IAEA-CN-38/X1.

[7] HAWRYLUK, R. J., SUCKEWER, S., and HIRSHMAN, S. P., Nuclear Fusion 19, 607 (1979).

[8] NRL Plasma Formulary, 1978, ed., Book, D. L., Naval Research Laboratory, Washington, D. C.

[9] POST, D. E., SINGER, C. E., and McKENNEY, A. M., Princeton Plasma Physics Laboratory Report 33, (1981).

[10] BUDNY, R., Private Communication.

[11] COHEN, S., Private Communication.

[12] SCHWEER, B., RUSBULDT, D., HINTZ, E., ROBERTO, J. B., and HUSINSKY, W. R., J. Nucl. Mat. 93, 357 (1980).

[13] ADAMCZYK, B., BOERBOOM, A. J. H., SCHRAM, B. L., and KISTEMAKER, J., J. Chem. Phys. 44, 4640 (1966).

[14] LOTZ, W., Ap. J. Suppl. 14, 202 (1967).

[15] RAPP, D., and ENGLANDER-GOLDEN, P., J. Chem. Phys. 43, 1465 (1965).

[16] MELTON, C. E., and RUDOLPH, P. S., J. Chem. Phys. 47, 1771 (1967).

[17] WINTERS, H. F., J. Chem. Phys. 63, 3462 (1975).

[18] DE HEER, F. J., Second Technical Committee Meeting on Atomic and Molecular Data for Fusion held at Fontenay-aux-Roses, FOM nr. 49 340, A.M.O.L.F. 80/115 (1980).

[19] HUNTRESS, W. T., Jr., Ap. J. Suppl. 33, 495 (1977).

[20] KOOPMAN, D. W., Phys. Rev. 178, 161 (1969).

[21] KOOPMAN, D. W., J. Chem. Phys. 49, 5203 (1968).

[22] McGOWAN, J. Wm., MUL, P. M., D'ANGELO, V. S., MITCHELL, J. B. A., DE FRANCE, P., and FROELICH, H. R., Phys. Rev. Lett. 42, 373 (1979).

[23] MUL, P. M., and McGOWAN, J. W., Ap. J. 237, 749 (1980).

[24] AUERBACH, R., CACAK, R., CAUDANO, R., GAILY, T. D., KEYSER, C. J., McGOWAN, J. W., MITCHELL, J. B. A., and WILK, S. F. J., J. Phys. B. 10, 3797 (1977).

[25] TUNITSKII, N. N., KUPRIYANOV, S. E., and PEROV, A. A., Bull. Acad. Sci. USSR, Chem. Ser. 11, 1857 (1962).

[26] PEART, B. and DOLDER, K. T., J. Phys. B 7, 1567, (1973); J. Phys. B 8, L143 (1975).

[27] LORQUET, A. J., LORQUET, J. C., WANKENNE, H., and MOMIGNY, J., J. Chem. Phys. 55, 4053 (1971).

[28] LOTZ, W., Z. f. Phys. 216, 241 (1968).

[29] BUTLER, S. E., and DALGARNO, A., Center for Astrophysics Series No. 1219 (1980).

[30] ALDROVANDI, S. M. V., and PEQUIGNOT, D., Astron. and Ap. 25, 137 (1973), and Errata 47, 321.

TABLE I

Collisional Reactions with Molecules: Cross Sections or Rate Constants

Reaction	$\sigma^{(1)}$ or $\langle\sigma v\rangle$ (cm^2 or $cm^3 s^{-1}$)
1. $e + CH_4 \rightarrow CH_4^+ + 2e$	$\sigma = 5.1 \times 10^{-15} E^{-1}[\ln(E/14) + \ln(E/30)]$
2. $e + CH_4 \rightarrow CH_3^+ + H + 2e$	$\sigma = 6.8 \times 10^{-15} E^{-1}[\ln(E/19) + \ln(E/30)]$
3. $e + CH_4 \rightarrow CH_3 + H + e$	$\sigma = 5.2 \times 10^{-15} E^{-1}[\ln(E/10) + 1.2 \ln(E/15)]$
4. $p + CH_4 \rightarrow CH_4^+ + H$	$\langle\sigma v\rangle = 5.5 \times 10^{-9} T_e^{1/2}$
5. $e + CH_4^+ \rightarrow CH_3 + H$	$\langle\sigma v\rangle = 6.3 \times 10^{-8} T^{-0.1}$, $T_e > 1$ eV
6. $e + CH_4^+ \rightarrow CH_3^+ + H + e$	$\sigma = 2.8 \times 10^{-14} E^{-1} \ln(E/15.8)$; $E > 15.8$
7. $e + CH^+ \rightarrow C^+ + H$	$\sigma = \alpha\sigma(CH_4^+)$
8. $e + CH^+ \rightarrow C + H^+$	$\sigma = (1 - \alpha)\sigma(CH_4^+)$
9. $e + CH^+ \rightarrow C + H$	$\langle\sigma v\rangle = 2.1 \times 10^{-8} T^{-0.1}$, $E > 1$ eV

(1) Where a term of the form $\ln(E/E_i)$ appears in σ, it is understood to apply only for $E > E_i$. For $E < E_i$, this term is zero.

TABLE II

Parameter	Δx From the Wall (cm)	
	Model 1	Model 2
Γ_{max}^{in}	6.7	13.5
$S_{max}(CH_4^+)$	3.9	11.5
$S_{max}(C^+,\ E = E_o)$	7.2	14.0
$S_{max}(C^+,\ E = E_f)$	9.5	18.0
$\ell_{toroidal}(max)$	16.0	24.0

TABLE III

Parameter	Δx From the Wall (cm)	
	Model 1	Model 2
$S_{max}(C \rightarrow C^{+}; E_o = 5\ eV)$	10.6	20.0
$S_{max}(CH_4 \rightarrow ..C^{+}; E_o = 0.03\ eV)$	9.5	18.0

FIGURE CAPTIONS

Fig. 1. The reaction rate constants are plotted as a function of temperature for the reactions of electrons and protons with methane and its derivatives.

Fig. 2. The equilbration time, τ_{eq}, and destruction time, 4 τ_d, for methane are compared as a function of temperature. These are plotted in units of $(\Sigma \langle \sigma v \rangle)^{-1}$, here denoted (tn) (the corresponding time is determined by dividing by n_e or n_p). Below 4 eV CH_n^+ equilibrates, while at higher energies a low energy ion gains some energy but does not equilibrate with the protons.

Fig. 3a. The density and temperature of the plasma in Model 1 are plotted as a function of distance away from the wall. These curves are taken from reference [7] and are based on a calculation using BALDUR [9]. The arrows indicate the location of the limiter.

Fig. 3b. The density and temperature of the plasma in Model 2 are plotted as a function of distance away from the wall. These curves are based on measurements and extrapolations for PDX in a standard D configuration. The arrows mark the location of the outer separatrix.

Fig. 4. The densities of CH_4 (solid line) and C (dashed line) are shown for particles leaving the wall. The flux of CH_4 corresponds to a density of 1 cm^{-3} and an energy of 0.03 eV at the wall; that for C is based on the same flux and energy (hence a slightly lower n at the wall due to the difference in velocities resulting from the mass differences). Model 1 is shown in Figure 4a and Model 2 in Figure 4b.

Fig. 5. The source functions for several species are plotted as a function of position for Models 1 and 2 (Figs. a and b, respectively). The curves for S (C^+, $E = E_o$) correspond to carbon leaving the wall with an energy E_o = 0.03 eV. Those for S (C^+, $E = E_f$) are the carbon ions produced in the plasma with the equilibration energy of the CH_n^+ ($E = E_f$). These latter source functions have one peak near that of S (CH^+) since some C^+ is produced directly from the dissociation of its precursor CH^+. The second peak is located deeper in the plasma and corresponds to the place where the energetic neutral carbon is ionized. In both models this peak in the source function is located further into the plasma than that due to carbon leaving the walls.

Fig. 6. The flux of carbon atoms produced in the plasma from CH_4 going into (Γ^{in}) and out of (Γ^{out}) the plasma are shown for Models 1 and 2 (Figs. a and b). Nearly half the carbon returns to the walls in both cases.

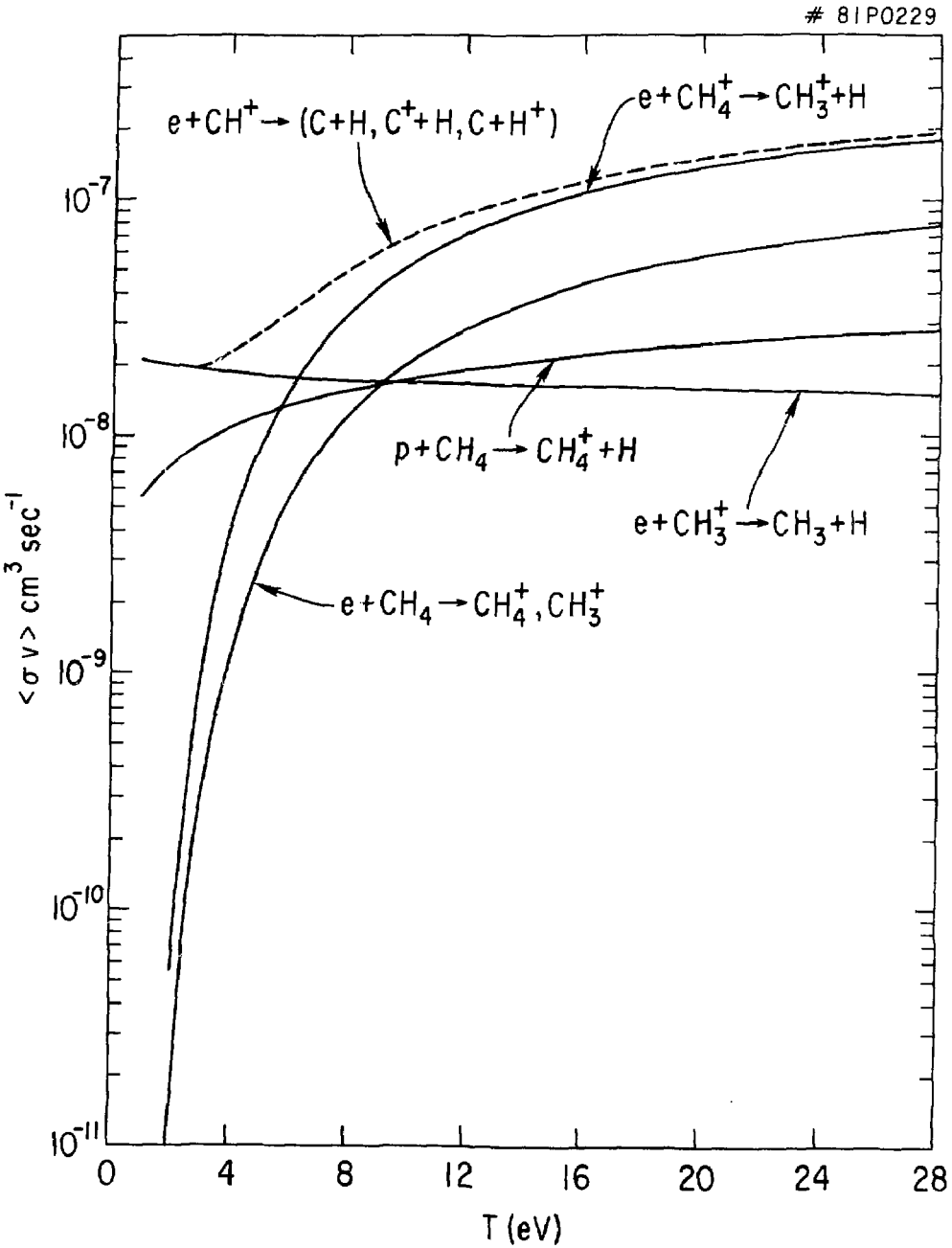
81P0229
e+CH+ → (C+H, C+ + H, C + H+)
e+CH4+ → CH3+ + H
p+CH4 → CH4+ + H
e+CH3+ → CH3 + H
e+CH4 → CH4+, CH3+
10-7
10-8
10-9
10-10
10-11
<σ v> cm3 sec-1
0
4
8
12
16
20
24
28
T (eV)

Fig. 1

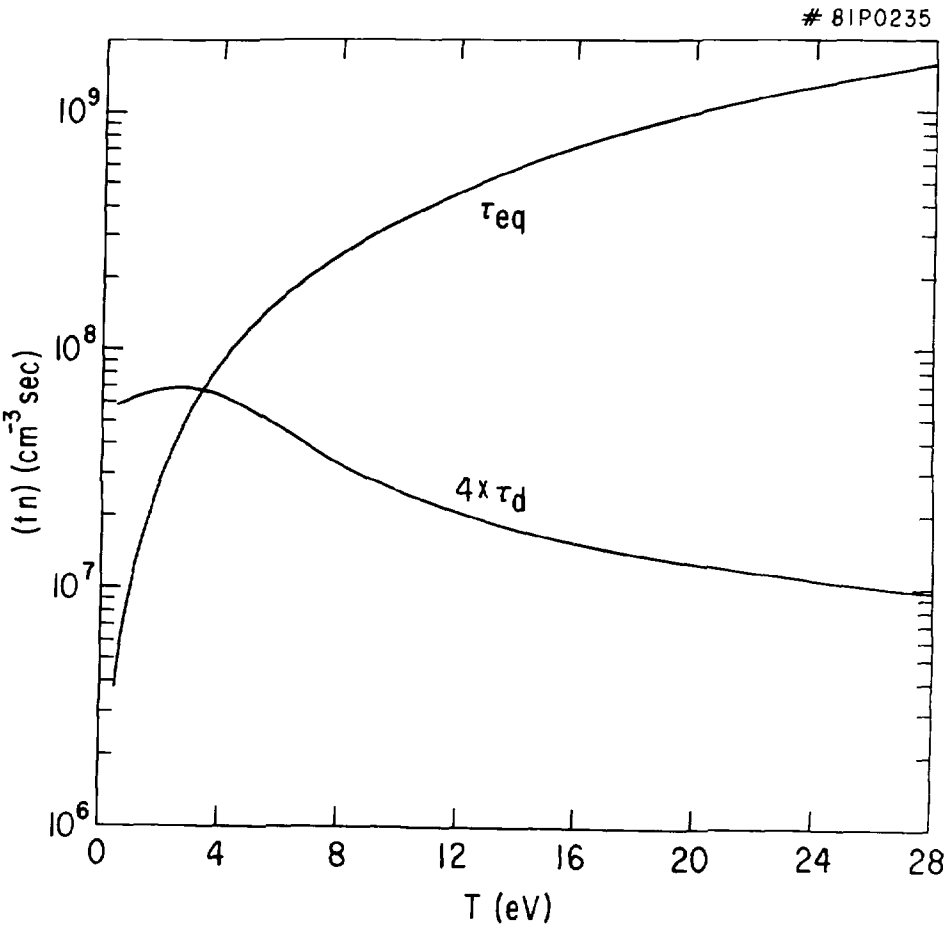
81P0235
10^9
10^8
10^7
10^6
$(t\,n)\ (cm^{-3}\,sec)$
τ_{eq}
$4 \times \tau_d$
0
4
8
12
16
20
24
28
T (eV)

Fig. 2

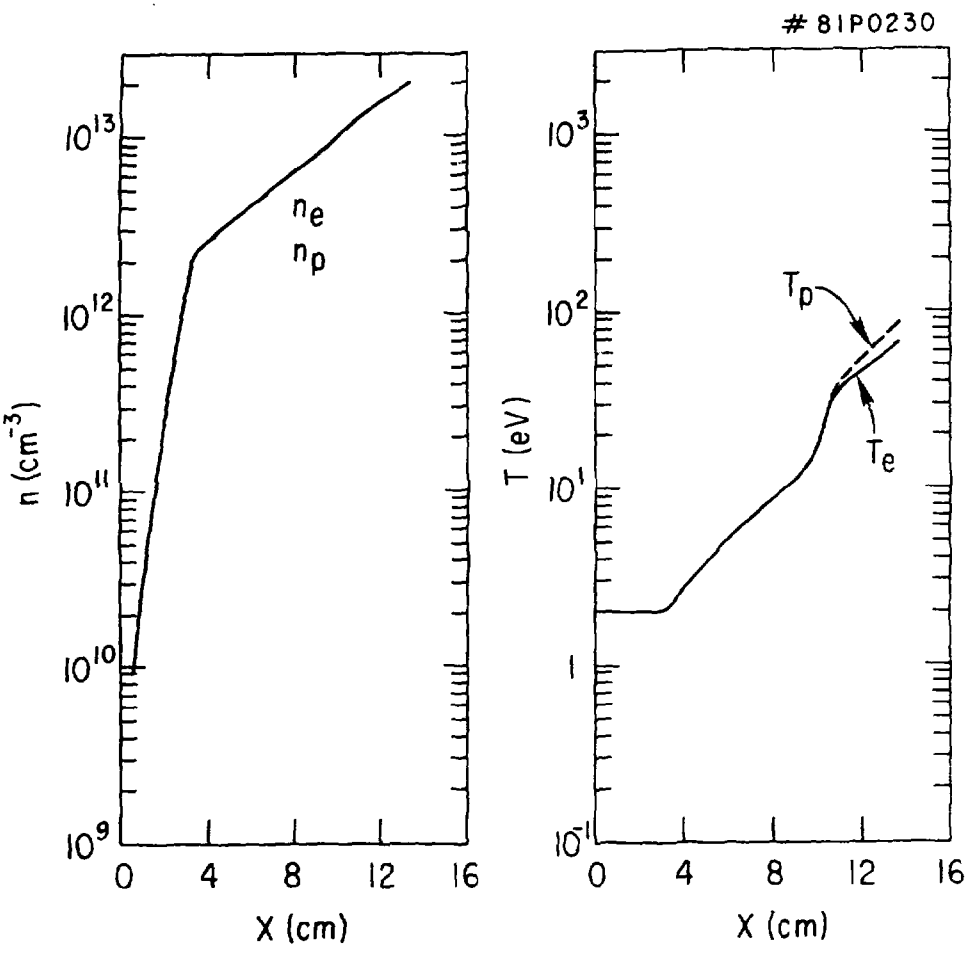
#81P0230
10^{13}
10^{12}
10^{11}
10^{10}
10^{9}
n (cm^{-3})
n_e
n_p
0
4
8
12
16
X (cm)
10^{3}
10^{2}
10^{1}
1
10^{-1}
T (eV)
T_p
T_e
0
4
8
12
16
X (cm)

Fig. 3a

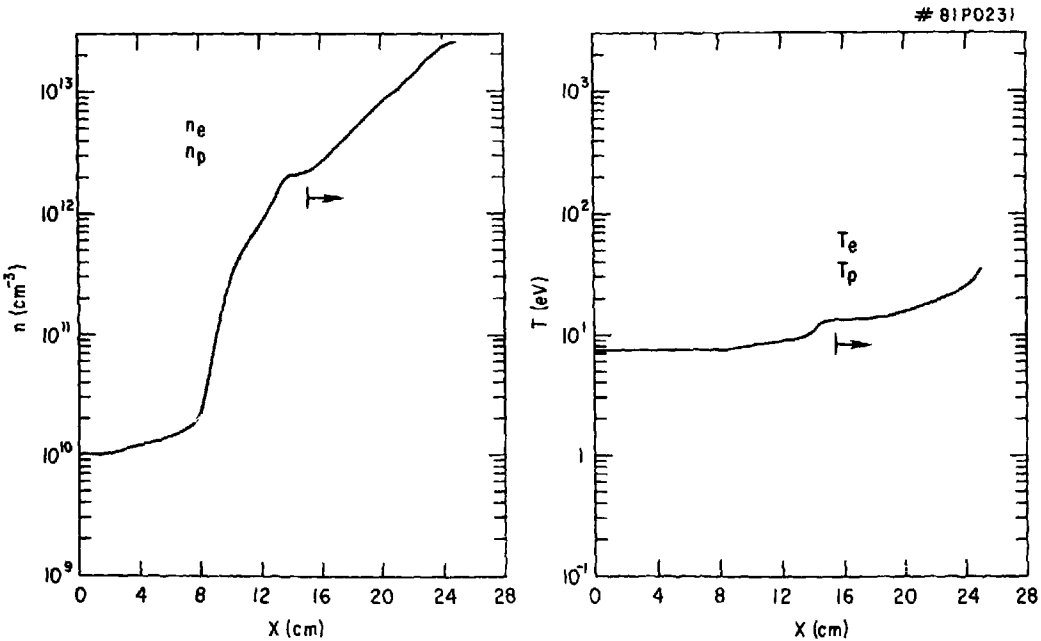
#81P0231
n_e
n_p
n (cm^{-3})
10^{13}
10^{12}
10^{11}
10^{10}
10^{9}
0
4
8
12
16
20
24
28
X (cm)
T_e
T_p
T (eV)
10^{3}
10^{2}
10^{1}
10^{-1}
0
4
8
12
16
20
24
28
X (cm)

Fig. 3b

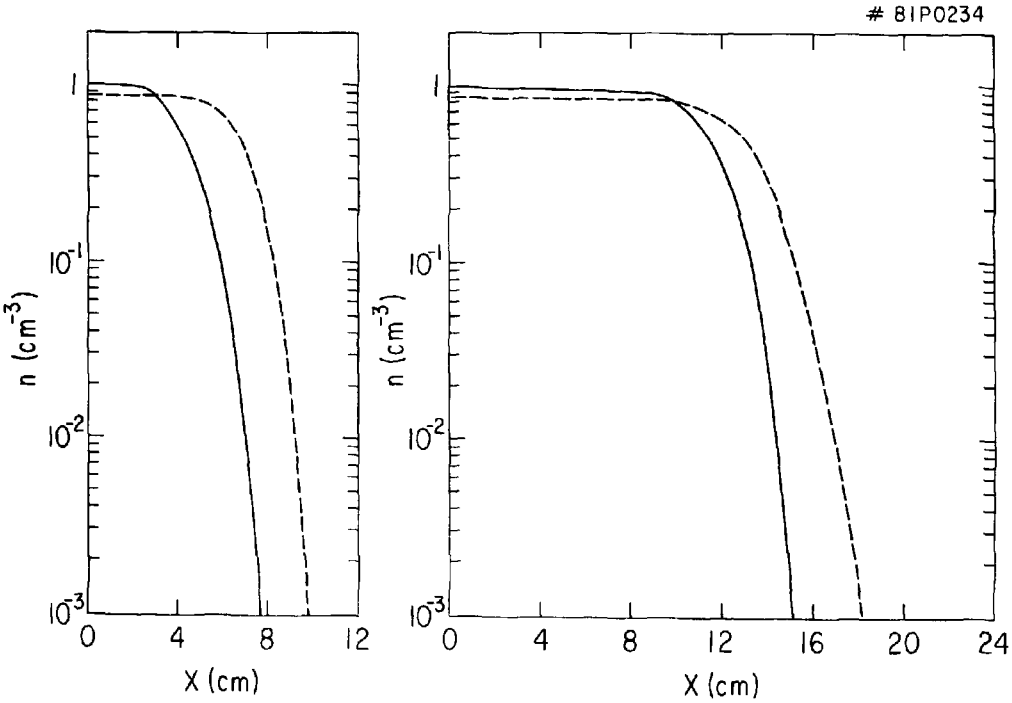

Fig. 4

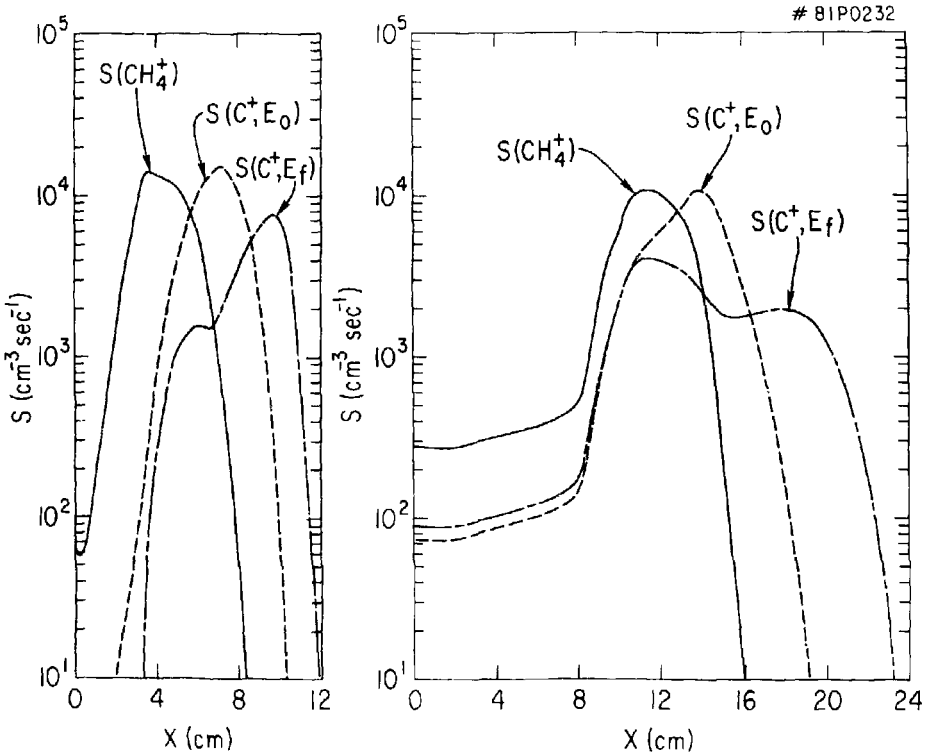
#81P0232
10^5
10^4
10^3
10^2
10^1
S (cm^{-3} sec^{-1})
S(CH$_4^+$)
S(C$^+$,E$_0$)
S(C$^+$,E$_f$)
0
4
8
12
16
20
24
X (cm)

Fig. 5

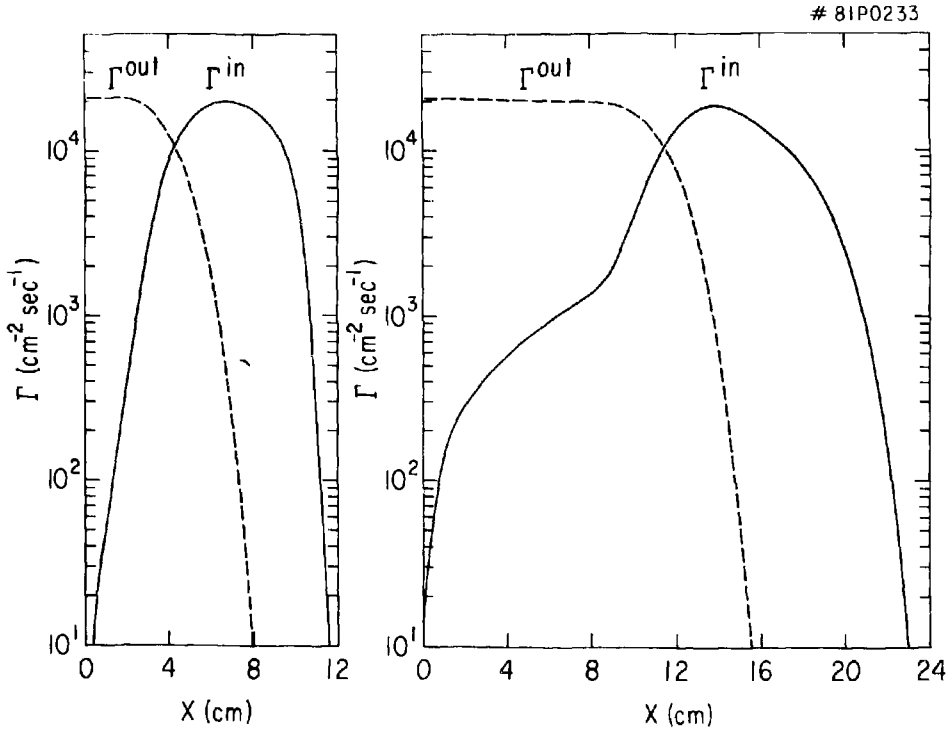
81P0233
Γ^{out}
Γ^{in}
Γ (cm^{-2} sec^{-1})
10^4
10^3
10^2
10^1
0
4
8
12
16
20
24
X (cm)

Fig. 6